Surv Geophys
DOI 10.1007/s10712-016-9381-3

Evaluation of the Global Mean Sea Level Budget between 1993 and 2014

Don P. Chambers[1] · Anny Cazenave[2,3] · Nicolas Champollion[3] · Habib Dieng[2] · William Llovel[4] · Rene Forsberg[5] · Karina von Schuckmann[6] · Yoshihide Wada[7]

Received: 21 December 2015 / Accepted: 22 July 2016

Abstract Evaluating global mean sea level (GMSL) in terms of its components—mass and steric—is useful for both quantifying the accuracy of the measurements and understanding the processes that contribute to GMSL rise. In this paper, we review the GMSL budget over two periods—1993 to 2014 and 2005 to 2014—using multiple data sets of both total GMSL and the components (mass and steric). In addition to comparing linear trends, we also compare the level of agreement of the time series. For the longer period (1993–2014), we find closure in terms of the long-term trend but not for year-to-year variations, consistent with other studies. This is due to the lack of sufficient estimates of the amount of natural water mass cycling between the oceans and hydrosphere. For the more recent period (2005–2014), we find closure in both the long-term trend and for month-to-month variations. This is also consistent with previous studies.

Keywords Sea level · Ocean mass · Steric sea level · Climate change

✉ Don P. Chambers
donc@usf.edu

[1] College of Marine Science, University of South Florida, 140 7th Ave. S, MSL119, St. Petersburg, FL 33701, USA

[2] Laboratoire d'Etudes en Géophysique et Océanographie Spatiales (LEGOS), 18 avenue Edouard BELIN, 31401 Toulouse Cedex 9, France

[3] International Space Science Institute (ISSI), Hallerstrasse 6, 3012 Bern, Switzerland

[4] Centre Européen de Recherche et de Formation Avancée en Calcul Scientifique (CERFACS), URA1875, 42 Avenue Gaspard Coriolis, 31057 Toulouse Cedex 1, France

[5] Division of Geodynamics, Technical University of Denmark, Elektrovej Building 327, room 022, 2800 Kgs., Lyngby, Denmark

[6] MERCATOR-Ocean, 10 Rue Hermès, 31520 Ramonville-Saint-Agne, France

[7] Department of Physical Geography, Utrecht University, P.O. Box 80115, 3508, TC, Utrecht, The Netherlands

Published online: 17 August 2016

1 Introduction

Sea level varies on a variety of spatial and temporal scales. Regionally, fluctuations in wind and currents can cause large deviations in sea level away from the global mean for periods of years to decades (e.g., Miller and Douglas 2007; Sturges and Douglas 2011; Chambers et al. 2012; Calafat and Chambers 2013; Palanisamy et al. 2015). One example of regional sea level change, from the tide gauge at Key West, Florida, is shown in Fig. 1, compared with an estimate of global mean sea level (GMSL) reconstructed from tide gauge records.

These large regional fluctuations, however, reflect mainly dynamical redistributions of heat and mass in the ocean and thus should average to zero when integrated over the global ocean. While the tide gauge network before the 1960s might not be sufficient to completely average these effects (see Fig. 8 in Calafat et al. 2014), satellite observations of sea surface height allow us to almost completely average out these internal variations and detect the smaller GMSL signal. These records show that GMSL has been rising at a rate between 2.8 and 3.6 mm year^{-1} between January 1993 and December 2014 (90 % confidence bands), with significant low-frequency variability superimposed (e.g., Nerem et al. 2010; Church et al. 2013; Ablain et al. 2015).

However, in order to predict future sea level rise, it is not sufficient to just determine the rate of rise of GMSL. One also needs to understand the mechanisms driving GMSL variability, and how they are changing in time. The primary mechanisms leading to current GMSL rise are: (1) water mass lost from ice sheets, glaciers, and ice caps that is gained by the oceans (e.g., Shepherd et al. 2012; Gardner et al. 2013), (2) volume (density) change due to thermal expansion as the oceans warm (e.g., Domingues et al. 2008; Levitus et al. 2012), and (3) changes in land water storage (e.g., Wada et al. 2012). Salinity changes due to land ice melt, river runoff, and changes in evaporation/precipitation increase have only second-order effects on the GMSL (e.g., Gregory and Lowe 2000). But in practice, as observations are not exactly global, salinity changes to density should also be accounted for when data are available. The combined effect of ocean temperature and salinity is

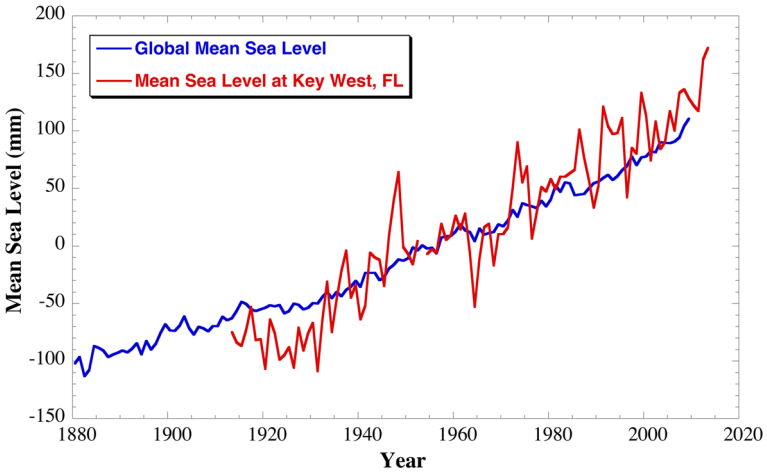

Fig. 1 Yearly averaged sea level change recorded by tide gauges at Key West, Florida compared to GMSL estimate from Church and White (2011). Tide gauge is from the Permanent Service for Mean Sea Level in Liverpool, UK

called the *steric* component, with the thermal contribution denoted *thermosteric*, and salinity contribution *halosteric*.

Because GMSL and estimates of the steric and mass components have different uncertainties and the potential for systematic errors, one often investigates the sea level budget to see how well it closes:

$$\mathrm{GMSL}(t) = \mathrm{GMSL}_{\mathrm{mass}}(t) + \mathrm{GMSL}_{\mathrm{steric}}(t). \quad (1)$$

At any particular time, t, the residual $(\mathrm{GMSL}(t) - \mathrm{GMSL}_{\mathrm{mass}}(t) - \mathrm{GMSL}_{\mathrm{steric}}(t))$ is unlikely to be exactly zero due to random and short-period errors. However, over the long-term, the residual differences should be small. When they are not, it indicates a problem in one or more of the terms in Eq. (1).

In addition, the mass and steric components are often subdivided into the various contributors. For mass, this includes separate estimates for contributions from the Greenland and Antarctica ice sheets, as well as from glaciers and ice caps. Exchanges of water mass between the oceans and the continents related to natural variability contribute significantly to seasonal and interannual contributions (e.g., Chambers et al. 2004; Llovel et al. 2011; Fasullo et al. 2013; Cazenave et al. 2014, Dieng et al. 2015a; Reager et al. 2016; Rietbroek et al. 2016), while storing water behind dams and extracting water from aquifers lead to non-negligible trends in GMSL (Chao et al. 2008; Konikow 2011; Pokhrel et al. 2012; Wada et al. 2012; Wada 2015; Dieng et al. 2015a).

Thermosteric changes are often separated into the upper ocean above 700 m, the layer between 700 and 1000 m, and the deeper ocean (e.g., Domingues et al. 2008; Purkey and Johnson 2010; Levitus et al. 2012). This is mainly an artifact of the older observing system, with substantially more observations in the upper ocean so that yearly averages could be obtained, whereas for the deeper layers, more temporal averaging is needed to extract the trend in the thermosteric component of GMSL. The halosteric component due to salinity changes is poorly known before the advent of the Argo observing system in the early 2000s (e.g., Durack et al. 2013), so typically, the halosteric contribution is neglected in sea level budget studies that include data from the 1990s (e.g., Domingues et al. 2008; Church et al. 2011). For this study, we also only consider the thermosteric sea level for the longer time period (1993–2015) and the steric sea level for the shorter time period (2005–2014).

One way to quantify the closure of the sea level budget is computing trends in GMSL and the various components over various periods of time, and summing these up to see if they match within the uncertainty (e.g., Church et al. 2011, 2013). However, with the advent of global measurements of ocean mass from the GRACE satellite mission (e.g., Johnson and Chambers 2013; Llovel et al. 2014) and ocean temperatures and salinity above 2000 m depth from Argo autonomous profiling floats (Llovel et al. 2014; von Schuckmann et al. 2014), one can now look at the closure on monthly time scales since 2005 (e.g., Dieng et al. 2015b, c for a recent review).

In this paper, we will review the closure of the sea level budget not only in terms of trends, but also in terms of the temporal variability of GMSL and its components. We utilize numerous estimates of GMSL from altimetry, as well as several estimates of the mass components and thermosteric change. These data sets have slightly different temporal sampling and filtering applied. To be consistent, we will utilize a common sampling and filtering scheme to all data. Trends are computed over the same time periods, and uncertainty is computed accounting for correlated signals in the residuals. We assess the closure of the sea level budget on two different time periods: January 1993 to December

2014 (a mixture of all measurements), and January 2005 to December 2014 (GRACE/Argo/altimetry only).

Section 2 will discuss the specific datasets used, filtering applied, and methods used to compute trends and uncertainty. Section 3 will summarize the level of closure of the sea level budget for the three time periods, and Sect. 4 will discuss the results.

2 Data and Methods

2.1 Satellite Altimetry

Products from six processing groups are available for the altimetry-based sea level time series:

1. Validation and Interpretation of Satellite Oceanographic (AVISO; http://www.aviso.altimetry.fr/en/data/products/ocean-indicators-products/actualitesindicateurs-des-oceansniveau-moyen-des-mersindexhtml.html);
2. University of Colorado (CU Release 5; http://sealevel.colorado.edu/).
3. National Oceanographic and Atmospheric Administration (NOAA; http://www.star.nesdis.noaa.gov/sod/lsa/SeaLevelRise/LSA_SLR_timeseries_global.php).
4. Goddard Space Flight Center (GSFC version 2; http://podaac-ftp.jpl.nasa.gov/dataset/MERGED_TP_J1_OSTM_OST_GMSL_ASCII_V2)
5. Commonwealth Scientific and Industrial Research Organization (CSIRO; www.cmar.csiro.au/sealevel/sl_data_cmar.html).
6. The CCI sea level data (ftp.esa-sealevel-cci.org/Products/SeaLevel-ECV/V1_11092012/), Ablain et al. (2015).

The first five sea level data sets are based on TOPEX/Poseidon, Jason-1 and Jason-2 data averaged over the 66°S–66°N domain, except for the CSIRO data averaged over 65°S–65°N. The CCI dataset is based primarily on TOPEX/Poseidon, Jason-1 and Jason-2, but also includes data from the Envisat, ERS-1, and ERS-2 altimeter missions after they have been adjusted to remove orbit error and biases relative to TOPEX/Poseidon, Jason-1 and Jason-2. For each product, a set of instrumental and geophysical corrections is applied (details are given on the websites of each data set). In addition, the effect of glacial isostatic adjustment (GIA) using the estimate proposed by Peltier (2004) is accounted for in each sea level time series except for the NOAA data set. Thus, we corrected the latter for the GIA effect, by adding 0.3 mm year^{-1} to the GMSL time series (Peltier 2004).

The sea level time series are obtained either by directly averaging the along-track sea surface height data (e.g., CU) or by first gridding the unevenly distributed along-track data and then performing grid averaging (e.g., AVISO and NOAA). In all cases, an area weighting is applied. In addition to the geographical averaging method, other differences exist between the GMSL data sets because of the applied geophysical and instrumental corrections and the number of satellites considered. Discussion on these differences can be found in Masters et al. (2012), Henry et al. (2014), and Ablain et al. (2015). Details on the exact corrections applied to the altimetry data are detailed on the webpages of each group.

Five of the time series used in this study cover the period January 1993–December 2014, but one (the CCI product) ends in December 2013. Figure 2 shows the GMSL time series, after removing an annual and semiannual sinusoids and smoothing with a 3-month running mean to reduce a 60-day erroneous signal (e.g., Masters et al. 2012). At shorter time scales (from sub-seasonal to multi-annual) significant discrepancies of several mm are

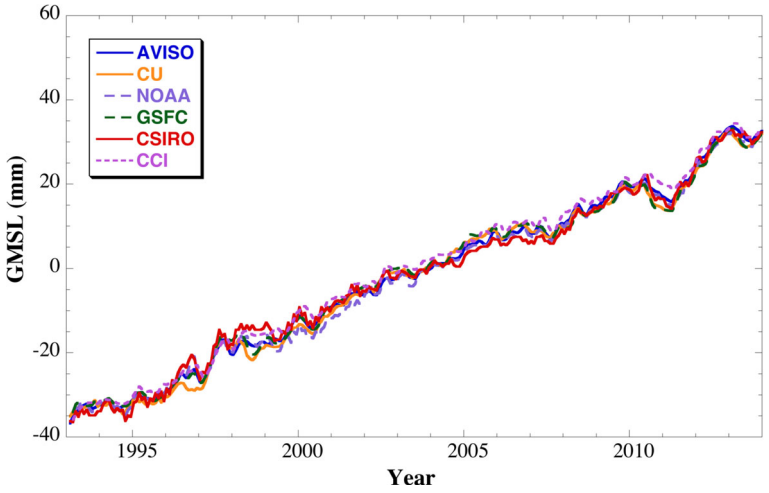

Fig. 2 GMSL from altimetry calculated by six different centers. Annual and semi-annual sinusoids have been estimated and removed, and a 3-month running mean filter has been applied

observed between the different GMSLs, especially between 2005 and 2008, and between mid-2010 and mid-2011, when there was a significant drop in GMSL related to changes in water storage over Australia and South America (Fasullo et al. 2013).

2.2 Steric Sea Level

Before the early 2000s, information on the steric sea level component comes from temperature data, due to the lack of global salinity data, coming primarily from expendable bathythermographs (XBTs), some mechanical bathythermographs (MBTs) and a much smaller number of conductivity-temperature-depth casts (CTDs) (e.g., Levitus et al. 2012; Abraham et al. 2013). The depth ranges of these instruments are very different, with XBTs mostly going only as deep as 700 m (although some go as deep as 1000–1500 m), while CTDs often make measurements to the sea floor. In the beginning of the 2000s, with the advent of the Argo program of autonomous floats (Roemmich et al. 2009), more measurements are available at more regular time intervals and also more globally. The current average density is approximately 1 float for every $3° \times 3°$ grid over the ocean. However, the depth to which Argo floats reach has also changed over time, starting at 1000 m, but now extending to 2000 m.

Computing steric sea level anomalies from these disparate data is not a trivial matter, but many groups have done so, using different interpolation and mapping methods, as well as different corrections for the XBT fall rate biases that have only recently been discovered (e.g., Gouretski and Koltermann 2007; Wijffels et al. 2008). Some groups use all available temperature data, while others restrict the estimate to only Argo data.

To quantify the steric component of GMSL change, we will consider different datasets. For the longer period (1993–2015), we will use two that merge XBTs, MBTs, CTDs, and Argo data, and provide the thermosteric sea level anomalies as a time series. They are:

1. NOAA data set, at https://www.nodc.noaa.gov/OC5/3M_HEAT_CONTENT (Levitus et al. 2012). The data are available as yearly averages of global mean thermosteric sea

level anomalies from the surface to 700 m depth, and 5-year running averages from the surface to 2000 m depth.

2. Domingues et al. (2008) version 3.1 dataset available from http://www.cmar.csiro.au/sealevel/thermal_expansion_ocean_heat_timeseries.html. The data are available as global mean thermosteric sea level anomalies from the surface to 700 m depth at yearly time steps but with a 3-year running mean filter applied.

To compare the two time series, we have applied a 3-year running mean to the NOAA time series (Fig. 3). Although the two estimates have similar long-term trends, there are substantial differences outside the authors' estimated standard errors at interannual periods. The biggest differences occur between 2000 and 2006, when the observing system is transitioning from mainly XBTs to mainly Argo floats. It has been shown that the different mapping techniques are highly sensitive to the mixture of the XBT/Argo data during this transition, partly due to small, unknown biases between different instrument types (Lyman and Johnson 2008; Lyman et al. 2010).

We use the Levitus et al. (2012) estimate of thermosteric sea level to 2000 m, available as 5-year running means, to estimate the thermosteric component between 700 and 2000 m depth. We reconstruct the signal between 700 and 2000 m by subtracting 5-year averages of the Levitus et al. (2012) 0–700 m time series. Uncertainty is that reported by the authors (after subtracting the uncertainty from 0 to 700 m assuming no correlation).

The only observations of deep thermosteric contributions are trends computed from deep hydrographic sections (Purkey and Johnson 2010; Kouketsu et al. 2011), estimated to be 0.11 ± 0.10 mm year^{-1} [uncertainty 95 % as reported by Purkey and Johnson (2010)] between approximately 1995–2005. We assume this value represents the trend for the entire period between 1993.0 and 2015.0.

After 2005, sufficient Argo floats are available to compute steric sea level anomalies from only these data (von Schuckmann et al. 2014; Roemmich et al. 2015). For this study, we utilize four different gridded datasets, providing temperature and salinity down to 2000 m depth at monthly intervals. They are:

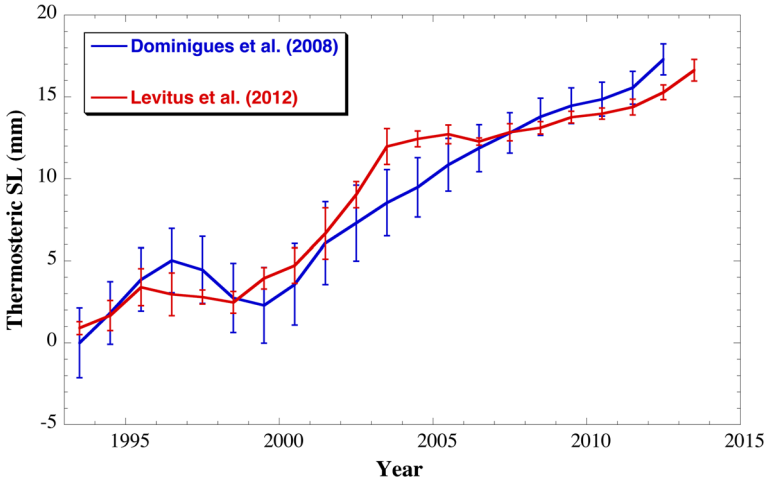

Fig. 3 Global mean thermosteric sea level contribution for upper ocean (0–700 m) from two analyses along with one standard error bars as computed by authors (Domingues et al. 2008; Levitus et al. 2012)

1. The International Pacific Research Center (IPRC; http://apdrc.soest.hawaii.edu/projects/Argo/data/Documentation/gridded-var.pdfhttp://apdrc.soest.hawaii.edu/projects/Argo/data/gridded/On_standard_levels/index-1.html)
2. The Japan Agency for Marine-Earth Science and Technology (JAMSTEC; ftp://ftp2.jamstec.go.jp/pub/argo/MOAA_GPV/Glb_PRS/OI/). Updated from Hosoda et al. (2008).
3. The SCRIPPS Institution of Oceanography (SCRIPPS; http://sio-argo.ucsd.edu/RG_Climatology.html). Updated from Roemmich et al. (2009).
4. The estimate from Karina von Schuckmann (KvS). Updated from Von Schuckmann and Le Traon (2011).

For the IPRC, JAMSTEC, and SCRIPPS data, we computed steric sea level time series from the surface down to 2000 m at monthly interval on a 1° × 1° grid for the period of January 2005 to December 2014 by integrating the density anomalies (defined as differences between the density estimate and a reference density at 0 °C and 35.16504 absolute salinity using the equation of state of seawater TEOS10 (http://www.teos-10.org/index.htm) at each standard depth. The KvS time series was computed using a similar methodology more fully described in von Schuckmann et al. (2009).

The Argo-based estimates of steric sea level since 2005 show similar decadal trends, but significantly different monthly and interannual variations (Fig. 4). Differences are of the order of 5 mm over some periods (2005 and 2010–2011, for example), but closer to 3 mm over other periods. The standard deviation of the differences ranges from a low of 1.5 mm between IPRC and JAMSTEC, to 2.9 mm between Scripps and JAMSTEC. IPRC and JAMSTEC also have the highest correlation of 0.92, while the correlation between Scripps and JAMSTEC, while still significant, is only 0.63. See Dieng et al. (2015b, c) for a detailed discussion on these differences.

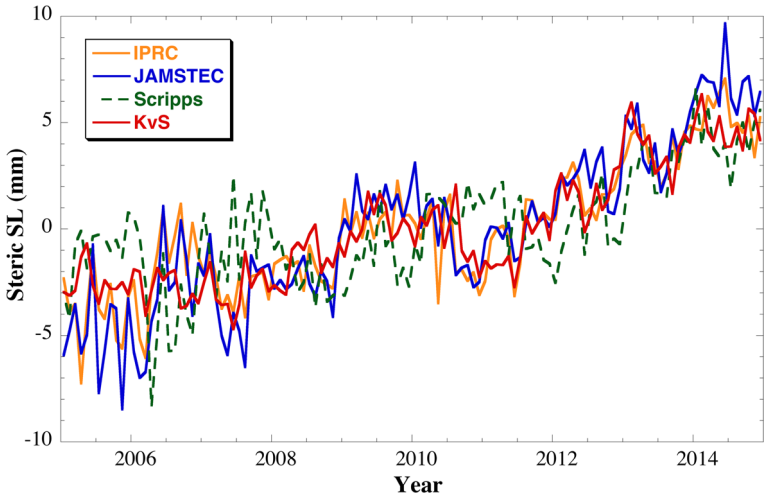

Fig. 4 Monthly estimates of global mean steric sea level anomalies (seasonal sinusoids removed) computed from Argo data from four processing centers

2.3 Satellite Gravity

The GRACE mission measures the Earth gravity field every month, generally released in terms of normalized spherical harmonic coefficients (Tapley et al. 2004), or more recently as gridded mass concentrations, or mascons (Watkins et al. 2015). One can convert the spherical harmonics into ocean mass variations in terms of an equivalent water thickness using either an averaging kernel approach (e.g., Chambers et al. 2004; Johnson and Chambers 2013), or more recently, by simply averaging the gridded mascons over the ocean domain (Watkins et al. 2015).

We utilize both approaches in this study and also use data from the three main processing centers—the Center for Space Research (CSR), the Helmholtz Centre Potsdam, German Research Centre for Geosciences (GFZ), and the Jet Propulsion Laboratory (JPL). JPL produces both spherical harmonics (SH) and mascons. Each center uses slightly different processing and analysis strategies, but many models and methods are similar. Thus, while comparison of the ocean mass from the various centers is instructive for quantifying a level of uncertainty, any systematic errors will not be obvious.

The data utilized are:

1. Averaging kernels from CSR, GFZ and JPL SH coefficients using the method described in Johnson and Chambers (2013), available from https://dl.dropboxusercontent.com/u/31563267/ocean_mass_orig.txt.
2. Averaging the JPL mascons (Watkins et al. 2015) over the global oceans, using an ocean mask that extends to the coastlines. The data are available from: http://grace.jpl.nasa.gov. Note that these data include a small signal from the global mean atmospheric pressure over the ocean, as explained in Johnson and Chambers (2013). This has been estimated and removed using the atmosphere model used to dealias the GRACE gravity data.

The differences between global mean ocean mass from the three centers and between spherical harmonics and mascons are small (Fig. 5). The biggest differences of order 5 mm

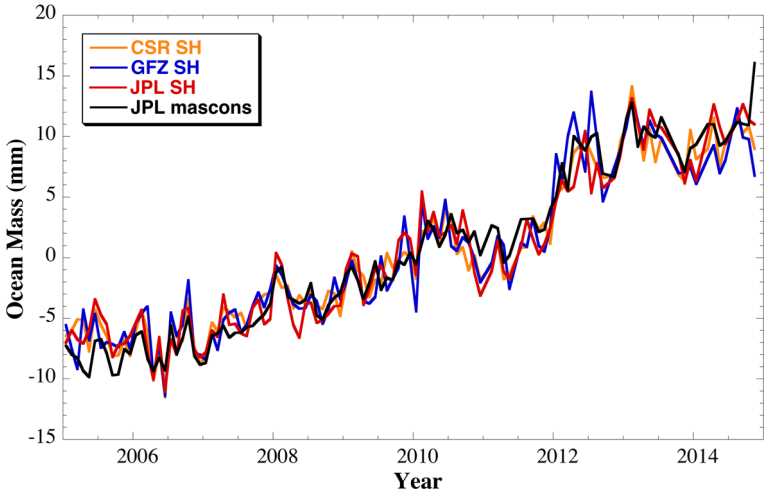

Fig. 5 Monthly estimate of global mean ocean mass anomalies (seasonal sinusoids removed) from GRACE computed by three different processing centers based on spherical harmonics (SH) and mascons

occur at the end and beginning of the records. The overall standard deviation of monthly differences is 1.6 mm.

2.4 Contributions from Ice Sheets and Glaciers

We consider contributions from the largest ice sheets (Greenland and Antarctica) separately from the glaciers and ice caps (GICs). The time series for Greenland and Antarctic mass balance comes from, for the longer period back to 1993, the synthesis of Shepherd et al (2012), based on surface mass balance models, synthetic aperture radar data, altimetry, and gravimetry (available from http://imbie.org/data-downloads/). For the shorter period since 2003, we use the estimates based only on GRACE computed by the group at the Technical University of Denmark (Sørensen and Forsberg 2010; Barletta et al. 2013).

GIC data come from an analysis of global glacier models driven by gridded climate observations, which has been shown to be consistent with extrapolations of in situ mass balance measurements (Marzeion et al. 2015).

2.5 Contributions from Land Hydrology

Ignoring the contribution from glaciers on continents, which is treated separately (Sect. 2.3), the land water contribution to sea level variation includes groundwater depletion, water impoundments behind dams, storage loss of endorheic lakes and wetlands, deforestation, and changes in soil moisture, permafrost and snow (i.e., natural water stores) (Church et al. 2011). Natural water storage change mostly varies with decadal climate variation and with insignificant trend on time periods greater than several decades (Ngo-Duc et al. 2005; Llovel et al. 2011), but can contribute to the trend on shorter periods (Cazenave et al. 2014). However, decomposing this signal is still a matter of significant research and fraught with uncertainties before GRACE observations are available starting in 2002, so we do not consider it for this study for the longer period 1993–2015.

Instead, we consider only estimates of groundwater depletion, water impoundment, deforestation, and the loss from large endorheic lakes. The contribution of groundwater depletion to GMSL is estimated using a flux-based method, i.e., calculating the difference between grid-based groundwater recharge (natural recharge and return flow from irrigation as additional recharge) and groundwater pumping (Wada et al. 2012; Wada 2015). This method, however, overestimates groundwater depletion for humid regions of the world. In order to correct the estimate, a global multiplicative correction factor is applied to the original estimate. The correction factor is based on a comparison between regionally reported groundwater depletion rates and simulated groundwater depletion rates (over 30 regions; Wada et al. 2012). An uncertainty analysis is performed with a Monte Carlo simulation, generating 100 equiprobable realizations of groundwater recharge and 100 equiprobable realizations of groundwater pumping, thus resulting in 10,000 possible realizations of groundwater depletion (assuming errors in groundwater recharge and groundwater abstraction to be independent) (Wada et al. 2012).

Water impoundment behind dams including additional storage in surrounding groundwater (through seepage) is based on the dataset of Chao et al. (2008). As this dataset only covers the period 1900–2007, it has been updated to include recently built dams including the Three Gorges dam and 250 other large dams up to the year 2011 (Wada et al. 2012). After the year 2011, the data are extrapolated. Deforestation rates are estimated from three different sources, averaged, and converted into a contribution to GMSL (Wada

et al. 2012). Wetland loss rate is estimated for USA where reported data are available, and then extrapolated the rate to rest of the world (Wada et al. 2012). Storage loss from endorheic basins is estimated only for the Aral and Caspian Seas (Wada et al. 2012).

2.6 Temporal Filtering and Combining Similar Data

The datasets previously discussed are provided with a range of temporal sampling, from monthly to yearly. Moreover, some have been filtered over longer times than they are sampled. For instance, the upper ocean thermosteric sea level estimate from Domingues et al. (2008) is provided at yearly time steps, but has had a 3-year running mean applied. The upper ocean thermosteric estimates from Levitus et al. (2012), on the other hand, are yearly averages. Thus, direct averaging of the two will lead to spurious differences related to the different smoothing applied.

Since one cannot unfilter a dataset, we are forced to utilize the longest filtering period among the datasets in order to make the time series as uniform as possible, and reduce the effect of unfiltered higher-frequency variability in some data. This means that yearly sampling and a 3-year running mean filter is applied to the time series that extend back to 1993, including the altimetry (Sect. 2.1), thermosteric (Sect. 2.2), ice contributions (Sect. 2.3), and hydrology components (Sect. 2.4). For the period 2005–2015, a monthly average is used, but the seasonal variation is estimated and removed by fitting a sinusoid term with annual (1 cycle per year, cpy) and semi-annual (2 cpy) frequencies using ordinary least squares in order to focus on only the interannual and longer variations. A 3-month running mean is also applied to be consistent with the smoothing used with the altimetry time series (Sect. 2.1).

When multiple datasets are available (e.g., altimetry GMSL, Argo thermosteric variations, GRACE ocean mass) the time series is averaged to compute an ensemble mean. Uncertainty is computed from the standard deviation of the residuals of the individual time series with the ensemble mean. This is assumed to be the standard error at each time step. For time series without multiple estimates, the uncertainty from the authors of the data is used. The total thermosteric signal is reconstructed from the ensemble average of the upper ocean time series (Fig. 3), the estimate from 700 to 2000 m based on Levitus et al. (2012), and the deep warming trend from Purkey and Johnson (2010). Standard errors in each component are added assuming they are uncorrelated by using a root-sum-square (RSS).

The satellite altimetry and GRACE observations also have a likelihood of unknown systematic errors that will affect the trend estimate. For altimetry, this arises from drifts and biases in the different instruments and the difficulty of detecting it through calibration with tide gauges, which also have vertical land motion that is often poorly measured (Mitchum 2000; Ablain et al. 2015; Watson et al. 2015). The full range of possible drift errors has previously been estimated to be between ± 0.4 mm year^{-1} (Mitchum 2000) and ± 0.5 mm year^{-1} (Ablain et al. 2015). More recently, Watson et al. (2015) found a higher possible change of 0.6 mm year^{-1} for the combined record. Here we use the value of ± 0.6 mm year^{-1} to be most conservative. This uncertainty is used for all time periods, even though Watson et al. (2015) argue it is considerably less for the Jason-1 and Jason-2 altimeters (post 2002). For GRACE, the uncertainty arises from uncertainty in the glacial isostatic adjustment (GIA) correction and has been estimated to be ± 0.3 mm year^{-1} (Chambers et al. 2010). These uncertainty values are added to those determined from the internal statistics (Sect. 2.6) using an RSS.

2.7 Fitting Trends and Computing Uncertainty

While trends do not give a complete picture of the sea level budget closure, they are a useful tool to detect imbalance and have been frequently used as a measure of the sea level budget closure (e.g., Church et al. 2011, 2013). We will fit a bias plus a trend ($a_0 + a_1 t$) model to each time series using ordinary least squares (OLS). Uncertainty estimates from ordinary least squares, however, assumes: (1) The uncertainty is proportional to the standard deviation of the residuals about the fit, (2) the uncertainty is proportional to 1/sqrt(N), where N is the number of points, and (3) the N points are statistically uncorrelated. In practice, these assumptions are rarely all true. For example, by temporally smoothing data, the points are not uncorrelated, and assumption (3) is violated. Assumption (1) is based on uncertainty arising from internal, unmodeled variability. But if this is smaller than the standard error of the estimate, the uncertainty in the trend will be underestimated.

There are several ways to deal with this issue and account for uncertainty properly. For small numbers of points (<20 or so), using Monte Carlo estimates with a colored noise model is not preferred, as it is difficult to compute the autocovariance of the data with such limited samples. This is the case for the longer time span when we have applied a 3-year mean filter. Instead, it is better to estimate the effective degrees of freedom (eDOF), which is the number of statistically independent observations minus the number of model parameters estimated (in the case of the 3-year smoothed data, it is only a bias + trend, so 2). In the case of the 3-year smoothed data between 1993 and 2015, we assume the points are uncorrelated after three years. The effective degrees of freedom for each data set are given in Table 1, noting they vary because the time lengths are slightly different.

Once the eDOF is known, it is straightforward to estimate the corrected uncertainty by

$$\sigma_{\text{corr}} = \sigma_{\text{OLS}} \sqrt{\frac{N}{e\text{DOF}}}, \tag{2}$$

Table 1 Estimated trends in GMSL and components between approximately January 1993 and December 2015

Quantity	Period	Trend (mm year^{-1})	Temporal averaging	Effective DOF
GMSL	1993–2015	3.19 ± 0.63[a]	3-year running means	5
Thermosteric				
0–700 m	1992.0–2014.0	0.85 ± 0.2	3-years	5
700–2000 m	1992.0–2014.0	0.24 ± 0.07	5-years	3
Below 2000 m	~1995–2005	0.11 ± 0.1	Trend only	N/A
Total thermosteric	~1992–~2014	1.20 ± 0.23	Sum of component trends	N/A
Antarctica	1992.0–2011.0	0.22 ± 0.14	3-years	4
Greenland	1992.0–2011.0	0.37 ± 0.28	3-years	4
Glaciers/ice caps	1992.0–2013.0	0.76 ± 0.30	3-years	5
Hydrology	1992.0–2013.0	0.45 ± 0.16	3-years	5
Total mass	~1992–~2013	1.8 ± 0.46		
Sum of components		3.00 ± 0.52		

Exact time period for each representative time series is given. Uncertainty is 90 % confidence except for the thermosteric below 2000 m, which is 95 % as estimated by Purkey and Johnson (2010)

[a] Includes uncertainty in knowing systematic drifts of ±0.6 mm year^{-1} (added as RSS)

where σ_{OLS} is the standard error from OLS based on the residuals and assuming N uncorrelated observations, and σ_{corr} is the corrected uncertainty by accounting for the smaller number of independent observations. However, the corrected uncertainty may still be too small, if the standard deviation of the residuals about the fit (used to scale the covariance matrix in OLS) is smaller than the prescribed standard errors for each observation (σ_{obs}). In this case, scaling the covariance matrix using the observation errors such as in weighted least squares (WLS) is better. Thus, to fully compute the most conservative uncertainty, we calculate both σ_{OLS} (based on the residuals to the fit) and σ_{WLS} (based on the observation errors) and derive σ_{corr} based on the greater of the two:

$$\sigma_{\mathrm{corr}} = \begin{bmatrix} \sigma_{\mathrm{OLS}}\sqrt{\dfrac{N}{e\mathrm{DOF}}}, & \text{if } \sigma_{\mathrm{OLS}} > \sigma_{\mathrm{WLS}} \\ \sigma_{WLS}\sqrt{\dfrac{N}{e\mathrm{DOF}}}, & \text{if } \sigma_{\mathrm{WLS}} > \sigma_{\mathrm{OLS}} \end{bmatrix}. \tag{3}$$

For the monthly sampled datasets between 2005 and 2015, we will use instead a Monte Carlo simulation based on a set of 10,000 simulated time series residuals that have an autocovariance similar to the true residuals. To do this, we use an auto-regression (AR) model to impose correlations to an initial random time series. An AR(p) model estimates values (y) at some time, t, based on p earlier times scaled by coefficients that had correlation:

$$y(t) = a_1 y(t-1) + a_2 y(t-2) + a_3 y(t-3) + \cdots + a_p y(t-p) + \varepsilon(t) \tag{4}$$

where $\varepsilon(t)$ is random noise with a prescribed variance.

The coefficients (a) are determined using the Yule-Walker algorithm, based on the one-sided autocovariance (i.e., where negative lags are treated the same as positive lags in the computation, assuming symmetry):

$$\begin{bmatrix} a_1 \\ a_2 \\ a_3 \\ \vdots \\ a_p \end{bmatrix} = \begin{bmatrix} R_0 & R_1 & \cdots & R_{p-1} \\ R_1 & R_0 & \cdots & R_{p-2} \\ \vdots & \vdots & \ddots & \vdots \\ R_{p-1} & R_{p-2} & \cdots & R_0 \end{bmatrix}^{-1} \begin{bmatrix} R_1 \\ R_2 \\ R_3 \\ \vdots \\ R_p \end{bmatrix} \tag{5}$$

$$\sigma_\varepsilon^2 = R_0 - \sum_{k=1}^{p} a_k R_k$$

R_0 is the autocovariance at lag=0, R_1 is the autocovariance at lag = 1, etc., and σ_ε is the standard deviation of the random noise needed to match the covariance at lag = 0.

Starting from 10,000 random time series with a standard deviation equal to that of the residuals, we derive and use the coefficients of an AR(3) model and create a 10,000 different colored noise models so that the covariance to lag-3 matches that of the original residuals. For the monthly sampled time series from 2005 to 2015, we do not consider the uncertainty of the observations, as the standard deviation of the residuals is higher than the observation error for all time series (altimetry, GRACE, Argo). We then fit trends to these simulated residuals, and the standard deviation of the 10,000 sample trends is used as one standard error for the trend uncertainty. This will properly inflate the uncertainty to account

for correlation in the time series. The degrees of freedom are computed from the autocorrelation of the time series, based on dividing the full time length in months by the decorrelation time, and rounding down. The decorrelation time is computed as twice the lag at which the autocorrelation drops below 0.5. The effective degrees of freedom are reduced by 6 (bias + trend, plus the previously estimated annual/semi-annual sinusoid).

All uncertainties are scaled to 90 % confidence, assuming a two-tailed *t*-distribution and accounting for the eDOF.

3 Results and Analysis

3.1 1993 to 2013

Figure 6 and Table 1 summarize the results of our assessment of the sea level budget from January 1993 to approximately December 2013. The end date is approximate, because several of the time series end earlier (notably the estimated from the Greenland and Antarctica ice sheets). The majority of the data have end dates in 2013.

Based on assessment of the trends over the 20-year interval (Table 1), the sea level budget closes within the uncertainty. The trend in GMSL is 3.19 ± 0.63 mm year^{-1}, while the trend in the sum of the components is 3.00 ± 0.52 mm year^{-1}. Thus, we have confidence that we understand the various contributors to GMSL rise over the last 20 years, at least within our current ability to measure them. The largest single contributor has been thermal expansion, explaining about 40 % of the trend (comparing relative to the sum of all components). The upper ocean alone explains about 28 % of the trend, with about 8 % coming from the middle layers, and 4 % from the deep ocean below 2000 m.

The contributors that combine to increase ocean mass, however, explain 60 % of the trend. Thus, the mass component of sea level rise between 1993 and 2014 was roughly 50 % greater than thermal expansion. Of the contributors, the glaciers and ice caps outside of Greenland and Antarctica had the largest effect (∼25 % of total GMSL), hydrology the

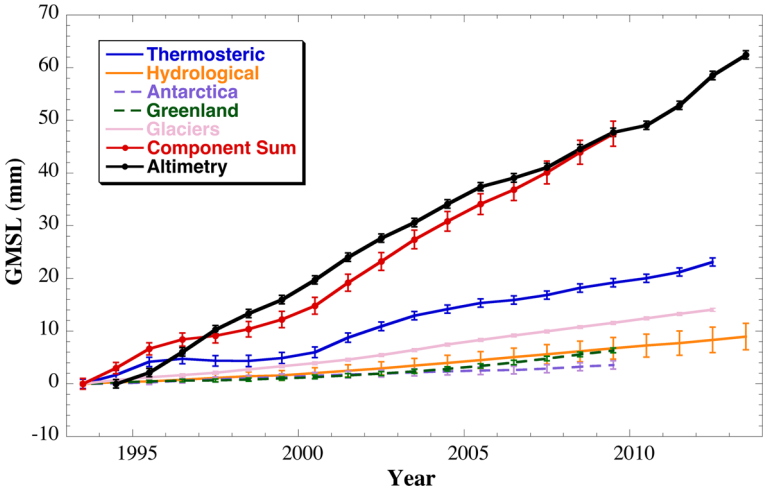

Fig. 6 Three-year running means of GMSL from altimetry, its components, and the sum of the components from 1993.0 to 2014.0. Uncertainty bars are one standard error as described in text

next (~15 %), then Greenland (~12 %), and finally Antarctica (~7 %). However, the contribution from Greenland has accelerated in recent years, as shown by several recent studies (e.g., Shepherd et al. 2012; Schrama et al. 2014; Velicogna et al. 2014; Yi et al. 2015). This is evidenced in Fig. 6 by the increasing separation between Greenland and Antarctica contributions. By 2010, the contribution to GMSL from Greenland has equaled the amount estimated from hydrological sources.

Although trends agree well, the time series of GMSL from altimetry and the sum of the components do not agree that well (Fig. 6). They disagree significantly at low frequencies. This is likely because our hydrological estimate does not include natural climate fluctuations in water cycling between the oceans and continents (Sect. 2.4). It is known that these signals on interannual (3- to 5-year time scales) can be of order 10 mm or so (e.g., Fasullo et al. 2013; Cazenave et al. 2014). These variations will be reflected in the GMSL estimate from altimetry, but not in the sum of the components.

3.2 2005 to 2014

Our ability to balance the sea level budget improves significantly after 2005 (Fig. 7; Table 2). Now, by measuring ocean mass directly from the satellite gravity measurements, we can observe similar low-frequency variability, for example, the significant drop of approximately 5 mm in 2011, followed by a subsequent rise of 16 mm between 2011 and 2013, followed by another 5 mm drop in late 2013 (Fig. 7). These are all related to exchanges of water mass between the oceans and continents and have only small steric sea level signatures. The perturbation in 2011 has been linked to anomalous rainfall over mainly Australia, with a lesser contribution from South America (Fasullo et al. 2013).

As with the 20-year period, the sea level budget over the last 10 years closes to within the uncertainty (Table 2). The rate in GMSL from altimetry is nearly unchanged from the 20-year estimate (3.17 ± 0.67 vs. 3.19 ± 0.63 mm year^{-1}). Although a few recent studies have found lower rates of GMSL over the last 10 years or so, these are affected by the

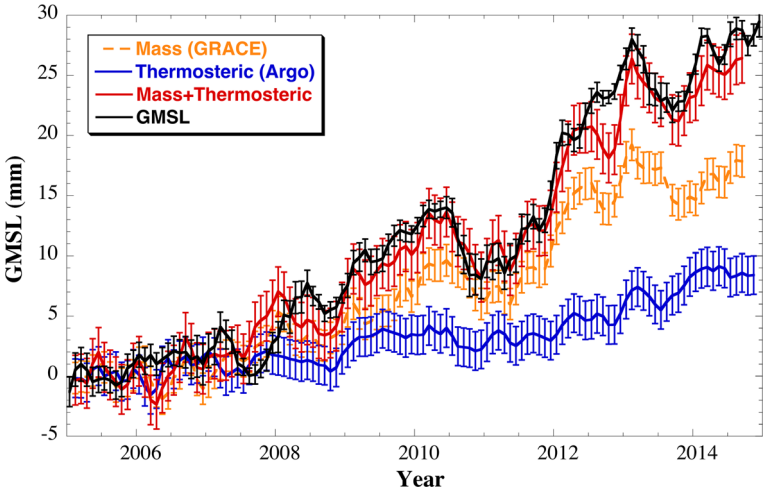

Fig. 7 Three-month running means of GMSL from altimetry, ocean mass from GRACE, and the thermosteric component from Argo for 2005.0–2015.0 (seasonal sinusoids removed). Time series are ensemble means and uncertainty *bars* are one standard error as described in text

Table 2 Estimated trends in GMSL and components between approximately January 2005 and December 2014 and from the representative time series

Quantity	Period	Trend (mm year^{-1})	Temporal averaging	Effective DOF
GMSL	2005.0–2015.0	3.17 ± 0.67[a]	3-month running mean	10
Thermosteric				
0–2000 m	2005.0–2015.0	0.86 ± 0.11	3-month running mean	10
Below 2000 m	~1995–2005	0.11 ± 0.1	Trend only	N/A
Total thermosteric	~2005–~2015	0.97 ± 0.15	Sum of component trends	N/A
Mass	2005.0–2015.0	2.11 ± 0.36[b]	3-month running mean	10
Sum of components		3.08 ± 0.39		

Exact time period for each representative time series is given. Uncertainty is 90 % confidence except for the thermosteric below 2000 m, which is 95 % as estimated by Purkey and Johnson (2010)

[a] Includes uncertainty in knowing systematic drifts of ±0.6 mm year^{-1} (added as RSS)

[b] Includes uncertainty in GIA of ±0.3 mm year^{-1} (added as RSS)

large interannual variability since 2011 (Cazenave et al. 2014). Earlier studies based on a scaling of El Niño indices suggested at least 15 years of data are necessary to distinguish longer term GMSL rise from that related to internal, natural variability (Nerem et al. 1999). Thus, one needs to be cautious of over-interpreting small changes in trends with short records.

The total steric contribution to GMSL is slightly smaller in the last decade than over the 20 years, while the mass component is slightly higher, although the means agree within uncertainty. Although we do not partition the ocean mass component into individual components from 2005 to 2014 due to limited degrees of freedom in the glacier and hydrology data, we do compare the relative contribution of Greenland and Antarctica mass loss (as measured by GRACE) to mean ocean mass (Fig. 8).

Over the last decade, the trend in Antarctica mass loss accounts for 3–27 % (central value 16 %) of the trend in global ocean mass, while Greenland accounts for 21–40 % (central value 32 %), when uncertainty is included in the possible spread. Greenland and Antarctica now account for about for 18–43 % (central value 28 %) of total GMSL rise, approximately the same amount as thermal expansion (25–56 %, central value 37 %). The contribution from glaciers and hydrology make up the remaining 35 %. Compare that to the period that includes the 1990s before the ice sheets began losing mass at an accelerated rate, when Greenland and Antarctica accounted for only ~20 % of the GMSL rate, while glaciers and hydrology accounted for ~40 %, based on the central values.

4 Conclusions

The results of this study are in agreement with previous estimates of the sea level budget (e.g., Church et al. 2011, 2013; Llovel et al. 2014; von Schuckmann et al. 2014; Dieng et al. 2015a, b, c). The main differences are in the slightly different time periods we study, along with what we consider more robust uncertainty estimates. The overall conclusion is that the sea level budget closes on both the longer (1993–2014) and shorter period (2005–2014) within the uncertainty. This gives us high confidence in the disparate measurements that go into the budget calculation. It also gives us increasing confidence that we

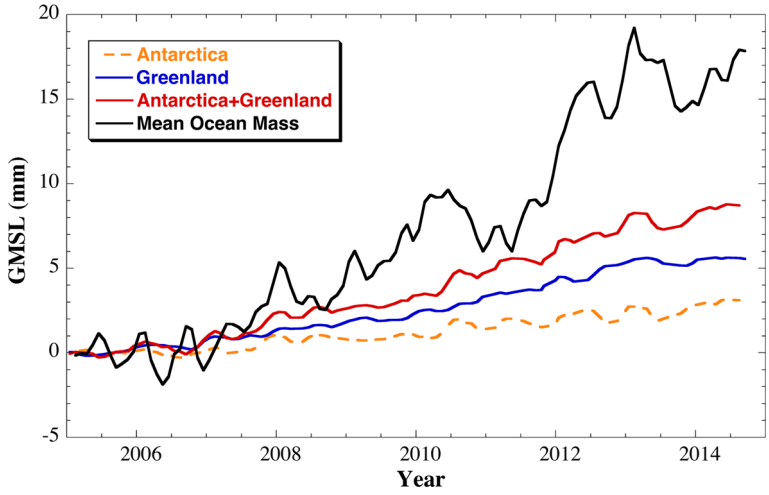

Fig. 8 Three-month running means of global mean ocean mass from GRACE, and the contributions from Greenland and Antarctica, also measured by GRACE

can partition the sources driving the observed rise in GMSL of $\sim$3.2 mm year^{-1}. From the sea level budget exercise, we know that thermal expansion drives about 40 % of the signal, with the majority of the expansion in the upper 700 m of the water column. Temperature changes in the deeper ocean, while smaller, still contribute significantly. Of the remaining 60 %, glaciers and ice caps outside of Greenland and Antarctica contribute the most ($\sim$25 % of total GMSL), Greenland and Antarctica ice sheets the next most (19 %), and hydrology the next ($\sim$15 %).

Over the last decade, the contributions from Greenland and Antarctica have accelerated considerably. Since 2005, Greenland has contributed 21 % of GMSL rise, while Antarctica has contributed 11 %. Combined, this is nearly a third of GMSL rise, and increase of nearly 68 % compared to the 20-year trend. The trend in GMSL over the two time intervals is roughly the same value ($\sim$3.2 mm year^{-1}). Thus, only by measuring the components of GMSL separately are we able to deduce changes in the mechanisms responsible for GMSL change, which allows us to better understand the processes.

These estimates, however, are based on the center of the possible spread of the trends. Unfortunately, we are still limited in reducing the spread due to potential systematic error in the observing system. The two largest uncertainties that have been documented are the inability to constrain the drift in altimeters to better than $\pm$0.6 mm year^{-1} and the GIA uncertainty on gravimetry estimates of ocean mass ($\pm$0.3 mm year^{-1}). As these are systematic, they will not be reduced by longer time series, unlike the error arising from unmodeled internal variability, which is reduced by a factor of 1/sqrt(n). Thus, concerted and continued efforts are needed to understand, measure, and correct systematic uncertainty in all portions of the observing system. Although the sea level budget closes to less than 0.2 mm year^{-1} (Tables 1, 2), this is just as likely to be a fortuitous cancellation of systematic errors as a real indication of accuracy.

Finally, it is vital to continue the observations of not only GMSL, but also the steric and mass components. Greenland and Antarctica contributions can be most directly observed via space-based gravimetry measurements, which provide an important constraint on other types of measurements (altimetry measurements of topography or input–output methods).

The independent Argo measurements confirm a slightly lower steric contribution, leaving no significant change in GMSL. In addition, expansion of the Argo measurements below 2000-m depth is important, as the only information we have from the deeper ocean are from more limited CTD casts. Although these are highly precise instruments, and deep ocean temperature/salinity are more correlated over larger regions, the low data availability results in uncertainty of order 50 %. Although the deep ocean is only a small contributor to sea level rise, as more heat is sequestered into the deeper ocean due to deep water formation, it may play an increasing role, considering that the volume of the deep ocean (below 2000 m) is nearly half that of the total ocean.

Acknowledgments This paper is the outcome of an International Space Science Institute Workshop (ISSI) "Integrative Study of Sea Level", and ISSI provided travel funding for the authors to attend the workshop. The Argo data were collected and made freely available by the International Argo Program and the national programs that contribute to it (http://www.argo.ucsd.edu and http://argo.jcommops.org). The Argo Program is part of the Global Ocean Observing System. DPC was supported by NASA Grant NNX12AL28G and internal funding from the University of South Florida. WL was supported by a CNES post-doctoral fellowship carried out at CERFACS. HD is supported by a doctoral fellowship of the European Space Agency within the Climate Change Initiative (CCI) Programme.

References

Ablain M, Cazenave A et al (2015) Improved sea level record over the satellite altimetry era (1993–2010) from the Climate Change Initiative Project. Ocean Sci 11:67–82. doi:10.5194/os-11-67-2015

Abraham JP et al (2013) A review of global ocean temperature observations: implications for ocean heat content estimates and climate change. Rev Geophys 51:450–483. doi:10.1002/rog.20022

Barletta VR, Sørensen LS, Forsberg R (2013) Scatter of mass changes estimates at basin scale for Greenland and Antarctica. Cryosphere 7:1411–1432. doi:10.5194/tc-7-1411-2013

Calafat FM, Chambers DP (2013) Quantifying recent acceleration in sea level unrelated to internal climate variability. Geophys Res Lett. doi:10.1002/grl.50731

Calafat FM, Chambers DP, Tsimplis MN (2014) On the ability of global sea level reconstructions to determine trends and variability. J Geophys Res Oceans 119:1572–1592. doi:10.1002/2013JC009298

Cazenave A, Dieng H, Meyssignac B, von Schuckmann K, Decharme B, Berthier E (2014) The rate of sea level rise. Nat Clim Chang 4:358–361. doi:10.1038/NCLIMATE2159

Chambers DP, Merrifield MA, Nerem RS (2012) Is there a 60-year oscillation in global mean sea level? Geophys Res Lett 39:L18607. doi:10.1029/2012GL052885

Chambers DP, Wahr J, Nerem RS (2004) Preliminary observations of global ocean mass variations with GRACE. Geophys Res Ltrs 31:L13310. doi:10.1029/2004GL020461

Chao BF, Wu YH, Li YS (2008) Impact of artificial reservoir water impoundment on global sea level. Science 320:212–214. doi:10.1126/science.1154580

Church JA, White NJ (2011) Sea-level rise from the late 19th to the early 21st century. Surv Geophys 32(4–5):585–602. doi:10.1007/s10712-011-9119-1

Church JA, White NJ, Konikow LF, Domingues CM, Cogley JG, Rignot E, Gregory JM, van den Broeke MR, Monaghan AJ, Velicogna I (2011) Revisiting the Earth's sea-level and energy budgets from 1961 to 2008. Geophys Res Lett 38:L18601. doi:10.1029/2011GL048794

Church JA, Clark PU, Cazenave A, Gregory JM, Jevrejeva S, Levermann A, Merrifield MA, Milne GA, Nerem RS, Nunn PD, Payne AJ, Pfeffer WT, Stammer D, Unnikrishnan AS (2013) Sea level change. In: Stocker TF, Qin D, Plattner G-K, Tignor M, Allen SK, Boschung J, Nauels A, Xia Y, Bex V, Midgley PM (eds) Climate Change 2013: The Physical Science Basis. Contribution of Working Group I to the Fifth Assessment Report of the Intergovernmental Panel on Climate Change. Cambridge University Press, Cambridge, UK and New York, NY, USA

Dieng H, Champollion N, Cazenave A, Wada Y, Schrama E, Meyssignac B (2015a) Total land water storage change over 2003–2013 estimated from a global mass budget approach. Environ Res Lett **(in press)**

Dieng H, Palanisamy H, Cazenave A, Meyssignac B, von Schuckmann K (2015b) The sea level budget since 2003: inference on the deep ocean heat content. Surv Geophys 36:1. doi:10.1007/s10712-015-9314-6

Dieng H, Cazenave A, von Shuckmann K, Ablain M, Meyssignac B (2015c) Sea level budget over 2005–2013: missing contributions and data errors. Ocean Sci 11:789–802. doi:10.5194/os-11-789-2015

Domingues CM, Church JA, White NJ, Gleckler PJ, Wijffels SE, Barker PM, Dunn JR (2008) Improved estimates of upper-ocean warming and multi-decadal sea-level rise. Nature 453:1090–1093

Durack PJ, Wijffels SE, Boyer TP (2013) Long-term salinity changes and implications for the global water cycle. In: Siedler G, Griffies SM, Gould J, Church JA (eds) Ocean circulation and climate, a 21st century perspective, 2nd edn. International Geophysics, Academic, Elsevier, Oxford, pp 727–757

Fasullo JT, Boening C, Landerer FW, Nerem RS (2013) Australia's unique influence on global mean sea level in 2010–2011. Geophys Res Lett 40(16):4368–4373. doi:10.1002/grl.50834

Gardner AS, Moholdt G, Cogley JG, Wouters B, Arendt AA, Wahr J, Berthier E, Hock R, Pfeffer WT, Kaser G, Ligtenberg SRM, Bolch T, Sharp MJ, Hagen JO, van den Broeke MR, Paul F (2013) A reconciled estimate of glacier contributions to sea level rise: 2003 to 2009. Science 340:852–857

Gouretski VV, Koltermann KP (2007) How much is the ocean really warming? Geophys Res Lett. doi:10.1029/2006GL027834

Gregory JM, Lowe JA (2000) Predictions of global and regional sea-level rise using AOGCMs with and without flux adjustment. Geophys Res Lett 27:3069–3072

Henry O, Ablain M, Meyssignac B, Cazenave A, Masters D, Nerem S, Leuliette E, Garric G (2014) Investigating and reducing differences between the satellite altimetry-based global mean sea level time series provided by different processing groups. J Geod 88:351–361. doi:10.1007/s00190-013-0687-3

Hosoda S et al (2008) A monthly mean dataset of global oceanic temperature and salinity derived 344 from Argo float observations. JAMSTEC Rep Res Dev 8:47–59

Johnson GF, Chambers DP (2013) Ocean bottom pressure seasonal cycles and decadal trends from GRACE release-05: ocean circulation implications. J Geophys Res Oceans. doi:10.1002/jgrc.20307

Konikow LF (2011) Contribution of global groundwater depletion since 1900 to sea-level rise. Geophys Res Lett 38:L17401. doi:10.1029/2011GL048604

Kouketsu S et al (2011) Deep ocean heat content changes estimated from observation and reanalysis product and their influence on sea level change. J Geophys Res Oceans 116:C03012

Levitus S, Antonov JI, Boyer TP, Baranova OK, Garcia HE, Locarnini RA, Mishonov AV, Reagan JR, Seidov D, Yarosh ES, Zweng MM (2012) World ocean heat content and thermosteric sea level change (0–2000 m), 1955–2010. Geophys Res Lett 39:L10603. doi:10.1019/2012GL051106

Llovel W, Becker M, Cazenave A, Jevrejeva S, Alkama R, Decharme B, Douville H, Ablain M, Beckley B (2011) Terrestrial waters and sea level variations on interannual time scale. Glob Planet Chang 75:76–82. doi:10.1016/j.gloplacha.2010.10.008

Llovel W, Willis JK, Landerer FW, Fukumori I (2014) Deep-ocean contribution to sea level and energy budget not detectable over the past decade. Nat Clim Chang. doi:10.1038/NCLIMATE2387

Lyman JM, Johnson GC (2008) Estimating annual global upper-ocean heat content anomalies despite irregular in situ ocean sampling. J Clim 21:5629–5641

Lyman JM, Good SA, Gouretski VV, Ishii M, Johnson GC, Palmer MD, Smith DA, Willis JK (2010) Robust warming of the global upper ocean. Nature 465:334–337. doi:10.1038/nature09043

Marzeion B, Leciercq PW, Cogley JG, Jarosch AH (2015) Brief communication: global glacier mass loss reconstructions during the 20th century are consistent. Cryosphere Discuss 9:3807–3820. doi:10.5194/tcd-9-3807-2015. www.the-cryosphere-discuss.net/9/3807/2015/

Masters D, Nerem RS, Choe C, Leuliette E, Beckley B, White N, Ablain M (2012) Comparison of global mean sea level time series from TOPEX/Poseidon, Jason-1, and Jason-2. Mar Geod 35:20–41

Miller L, Douglas BC (2007) Gyre-scale atmospheric pressure variations and their relation to 19th and 20th century sea level rise. Geophys Res Lett 34:L16602. doi:10.1029/2007GL030862

Mitchum GT (2000) An improved calibration of satellite altimetric heights using tide gauge sea levels with adjustment for land motion. Marine Geodesy 23:145–166

Nerem RS, Chambers DP, Choe C, Mitchum GT (2010) Estimating mean sea level change from the TOPEX and Jason altimeter missions. Mar Geod 33(Supplement 1):435–446. doi:10.1080/01490419.2010.491031

Nerem RS, Chambers DP, Leuliette E, Mitchum GT, Giese BS (1999) Variations in global mean sea level during the 1997–98 ENSO event. Geophys Res Ltrs 26:3005–3008

Ngo-Duc T, Laval K, Polcher J, Lombard A, Cazenave A (2005) Effects of land water storage on global mean sea level over the past 50 years. Geophys Res Lett 32:L09704. doi:10.1029/2005GL022719

Palanisamy H, Cazenave A, Delcroix T, Meyssignac B (2015) Spatial trend patterns in Pacific Ocean sea level during the altimetry era : the contribution of thermocline depth change and internal climate variability. Ocean Dyn. doi:10.1007/s10236-014-0805-7

Peltier WR (2004) Global glacial isostasy and the surface of the ice-age Earth: the ICE-5G (VM2) model and GRACE. Annu Rev Earth Planet Sci 32:111–149

Pokhrel YN, Hanasaki N, Yeh PJ-F, Yamada T, Kanae S, Oki T (2012) Model estimates of sea level change due to anthropogenic impacts on terrestrial water storage. Nat Geosci 5:389–392. doi:10.1038/ngeo1476

Purkey SG, Johnson GC (2010) Warming of global abyssal and deep Southern Ocean waters between the 1990 s and 2000 s: contributions to global heat and sea level rise budgets. J Clim 23:6336–6351

Reager JT, Gardner AS, Famiglietti JS, Wiese DN, Eicker A, Lo M-H (2016) A decade of sea level rise slowed by climate driven hydrology. Science 351:699–703. doi:10.1126/science.aad8386

Rietbroek R, Brunnabend SE, Kushche J, Schröter J, Dahle C (2016) Revisiting the contemporary sea-level budget on global and regional scales. Proc Natl Acad Sci 113:1504–1509. doi:10.1073/pnas.1519132113

Roemmich D, Johnson GC, Riser S, Davis R, Gilson J, Owens WB, Garzoli SL, Schmid C, Ignaszewski M (2009) The Argo program: observing the global ocean with profiling floats. Oceanography 22(2):34–43. doi:10.5670/oceanog.2009.36

Roemmich D, Church J, Gilson J, Monselesan D, Sutton P, Wijffels S (2015) Unabated planetary warming and its ocean structure since 2006. Nat Clim Chang 5:240–245

Schrama EJO, Wouters B, Rietbroek R (2014) A mascon approach to assess ice shett and glacier mass balance and their uncertainties from GRACE data. J Geophys Res Solid Earth 119:6048–6066. doi:10.1002/2013JB010923

Shepherd A et al (2012) A reconciled estimate of ice-sheet mass balance. Sci 338(6111):1183–1189

Sørensen LS, Forsberg R (2010) Greenland ice sheet mass loss from GRACE monthly models. In: Gravity, Geoid and Earth Observation. Springer. (International Association of Geodesy Symposia; No. 135), pp 527–532. doi:10.1007/978-3-642-10634-7_70

Sturges W, Douglas BC (2011) Wind effects on estimates of sea level rise. J Geophys Res 116:C06008. doi:10.1029/2010JC006492

Tapley BD, Bettadpur S, Watkins M, Reigber C (2004) The gravity recovery and climate experiment: mission overview and early results. Geophys Res Lett 31:L09607. doi:10.1029/2004GL019920

Velicogna I, Sutterley TC, van den Broeke MR (2014) Regional acceleration in ice mass loss from Greenland and Antarctica using Grace time variable gravity data. Res Lett Geophys. doi:10.1002/2014GL061052

Von Schuckmann K, Le Traon PY (2011) How well can we derive Global Ocean indicators from Argo data? Ocean Sci 7(6):783–791. doi:10.5194/os-7-783-2011

Von Schuckmann K, Gaillard F, Le Traon P-Y (2009) Global hydrographic variability patterns during 2003–2008. J Geophys Res 114:C09007. doi:10.1029/2008JC005237

Von Schuckmann K, Sallée JB, Chambers D, Le Traon PY, Cabanes C, Gaillard C, Speich S, Hamon M (2014) Consistency of the current global ocean observing systems from an Argo perspective. Ocean Sci 10:547–557. doi:10.5194/os-10-547-2014

Wada Y (2015) Modelling groundwater depletion at regional and global scales: Present state and future prospects. Surv Geophys. doi:10.1007/s10712-015-9347-x, Special Issue: ISSI Workshop on Remote Sensing and Water Resources

Wada Y, van Beek LPH, Sperna-Weiland FC, Chao BF, Wu Y-H, Bierkens MFP (2012) Past and future contribution of global groundwater depletion to sea-level rise. Geophys Res Lett 39:L09402. doi:10.1029/2012GL051230

Watkins MM, Wiese DN, Yuan D-N, Boening C, Landerer FW (2015) Improved methods for observing Earth's time variable mass distribution with GRACE. J Geophys Res Solid Earth. doi:10.1002/2014JB011547

Watson CS, White NJ, Church JA, King MA, Burgette RJ, Legresy B (2015) Unabated global mean sea-level rise over the satellite altimeter era. Nat Clim Chang 5(6):565. doi:10.1038/nclimate2635

Wijffels SE, Willis J, Domingues CM, Barker P, White NJ, Gronell A, Ridgway K, Church JA (2008) Changing expendable bathythermograph fall rates and their impact on estimates of thermosteric sea level rise. J Clim 21:56575672. doi:10.1175/2008JCLI2290.1

Yi S, Sun W, Heki K, Qian A (2015) An increase in the rate of global mean sea level rise since 2010. Geophys Res Lett. doi:10.1002/2015GL063902